

The UV-optical Color Gradients in Star-Forming Galaxies at $0.5 < z < 1.5$: Origins and Link to Galaxy Assembly

F. S. Liu^{1,2}, Dongfei Jiang^{1,3}, Yicheng Guo², David C. Koo², S. M. Faber², Xianzhong Zheng³, Hassen M. Yesuf², Guillermo Barro^{2,4}, Yao Li¹, Dingpeng Li¹, Weichen Wang⁵, Shude Mao⁵, and Jerome J. Fang^{2,6}

Email: fsliu@synu.edu.cn

¹*College of Physical Science and Technology, Shenyang Normal University, Shenyang 110034, China*

²*University of California Observatories and the Department of Astronomy and Astrophysics, University of California, Santa Cruz, CA 95064, USA*

³*Purple Mountain Observatory, Chinese Academy of Sciences, 2 West-Beijing Road, Nanjing 210008, China*

⁴*Department of Astronomy, University of California, Berkeley, CA 94720-3411, USA*

⁵*Department of Physics, Tsinghua University, Beijing 100084, China*

⁶*Orange Coast College, Costa Mesa, CA 92626, USA*

ABSTRACT

The rest-frame UV-optical (i.e., $NUV - B$) color index is sensitive to the low-level recent star formation and dust extinction, but it is insensitive to the metallicity. In this Letter, we have measured the rest-frame $NUV - B$ color gradients in ~ 1400 large ($r_e > 0.18''$), nearly face-on ($b/a > 0.5$) main-sequence star-forming galaxies (SFGs) between redshift 0.5 and 1.5 in the CANDELS/GOODS-S and UDS fields. With this sample, we study the origin of UV-optical color gradients in the SFGs at $z \sim 1$ and discuss their link with the buildup of stellar mass. We find that the more massive, centrally compact, and more dust extinguished SFGs tend to have statistically more negative raw color gradients (redder centers) than the less massive, centrally diffuse, and less dusty SFGs. After correcting for dust reddening based on optical-SED fitting, the color gradients in the low-mass ($M_* < 10^{10} M_\odot$) SFGs generally become quite flat, while most of the high-mass ($M_* > 10^{10.5} M_\odot$) SFGs still retain shallow negative color gradients. These findings imply that dust reddening is likely the principal cause of negative color gradients in the low-mass SFGs, while both increased central dust reddening and buildup of compact old bulges are likely the origins of negative color gradients in the high-mass SFGs. These findings also imply that at these redshifts the low-mass SFGs buildup their stellar masses in a self-similar way, while the high-mass SFGs grow inside out.

1. Introduction

Investigating the spatial distributions of galaxy properties (i.e., color, stellar mass, star formation rate, etc.) is a powerful way to understand the buildup and shutdown of galaxies. Color gradient can provide information on the stellar population within a galaxy, through its dependency on the galactic distributions of dust, stellar age and metallicity (Gonzalez-Perez et al. 2011; Guo et al. 2011). In the local universe, early-type galaxies (ETGs) are generally old and dead, containing relatively little or no dust and usually have negative optical and near-infrared color gradients (redder centers). Previous studies (e.g., Wu et al. 2005; Tortora et al. 2010) have shown that metallicity and not age gradients are the principal origin of such color gradients. Although color gradients in nearby late-type galaxies (LTGs) appear to be dominated by the fact that, on average, their bulges are redder than their disks, LTGs show age, metallicity and dust gradients, due to the interplay among dust content, stellar feedback, bursts of star formation and stellar migration (Gonzalez-Perez et al. 2011). Earlier studies have claimed a weak correlation of color gradients with the physical properties of local galaxies (e.g. mass, luminosity, etc., Peletier et al. 1990; Kobayashi & Arimoto 1999; Tamura & Ohta 2003), Recent studies on the basis of larger and homogeneous samples of galaxies in SDSS have found that color gradients in local galaxies are closely correlated with their stellar masses, luminosities, sizes, and residual star formation (e.g., Tortora et al. 2010; Suh et al. 2010; Pan et al. 2015). These results have provided important information on the physical origin of color gradients in local galaxies and clues on their buildup and shutdown.

At moderate and high redshifts, the relationship between color gradient and galaxy properties have not been fully explored to date. By stacking the *HST* multi-band imaging, Wuyts et al. (2012) studied the resolved colors and stellar populations of a few hundred star-forming galaxies (SFGs) with $M_* > 10^{10} M_\odot$ at $0.5 < z < 2.5$. They found evidence for redder color, lower star formation rate (SSFR), and increased dust extinction in the centers of galaxies, which are consistent with an inside-out disk growth scenario in massive SFGs. In a series of papers by Nelson et al. (i.e., Nelson et al. 2012,2015,2016), they studied the spatial map of SSFR traced by $H\alpha$ and dust map in SFGs at moderate redshifts ($z \sim 1$ and $z \sim 1.4$). Nelson et al. (2012) showed that the $H\alpha$ sizes of massive galaxies are bigger than their sizes in the rest-frame R-band. Nelson et al. (2015) showed that the $EW(H\alpha)$ is flat with radius for the low-mass ($\log M_*/M_\odot = 9.0 - 9.5$) galaxies, while the $EW(H\alpha)$ decreases by a factor of ~ 2 on average from center to $2r_e$ for high mass galaxies. These findings suggested that massive SFGs build up their stellar masses from inside out, while the low-mass SFGs grow in a self-similar way, irrespective of the radial distance. Note that dust correction was not done in these two works. So the results may be due to either lower central SSFR or higher central dust or combination of both in massive galaxies. Nelson et al. (2016)

corrected for dust-extinction by using the Balmer decrement ($H\alpha/H\beta$). As a result, central dust was found as a major factor in causing radial color gradient in galaxies with a mean mass of $\langle \log M_*/M_\odot \rangle = 10.2$. Galaxies with $\langle \log M_*/M_\odot \rangle = 9.2$ have little dust attenuation at any radii. These studies suggest that both dust and stellar population changes can result in a significant radial color gradient in a SFG at moderate redshift.

To a large extent, the degeneracies among the effects of dust, stellar age and metallicity on color gradients are hard to disentangle without independent information. However, metallicity usually affects the color of redder stars more strongly than the color of bluer ones. So it has been demonstrated successfully that, for the study of color gradients in local ETGs with little dust, including rest-frame near-infrared data is helpful to break the age-metallicity degeneracy (e.g., Wu et al. 2005). On the other hand, it has also been shown that the rest-frame UV-optical color index is sensitive to the low-level recent star formation (i.e., SSFR) and dust extinction, but is insensitive to the metallicity (e.g., Kaviraj et al. 2007; Pan et al. 2015; Fang et al. in prep.). In this Letter, we exploit deep high-resolution *HST*/WFC3 and ACS multi-band imaging data to measure the rest-frame $NUV - B$ color gradients for a sample of ~ 1400 SFGs near the ridge-line of the main sequence (MS), with $\log M_*/M_\odot > 10^9$ at $0.5 < z < 1.5$ selected from the CANDELS/GOODS-S and UDS fields. These data allow us to make a statistically robust analysis of UV-optical color gradients in actively SFGs at moderate redshifts. We examine the effects of dust and bulge formation on color gradients in SFGs and further discuss the link between color gradient and the stellar mass assembly.

Throughout the Letter, we adopt a cosmology with a matter density parameter $\Omega_m = 0.3$, a cosmological constant $\Omega_\Lambda = 0.7$ and a Hubble constant of $H_0 = 70 \text{ km s}^{-1} \text{ Mpc}^{-1}$. All magnitudes are in the AB system.

2. DATA

The sample of galaxies used in this work is selected from the first two available fields (GOODS-S & UDS) of the CANDELS (Grogin et al. 2011; Koekemoer et al. 2011). Based on the source detection in the WFC3/F160W band, the CANDELS team has made a multi-wavelength catalog for each field, combining the newly obtained CANDELS *HST*/WFC3 data with existing public ground-based and space-based data. *HST* photometry was measured by running **SExtractor** (Bertin & Arnouts 1996) on the point spread function (PSF)-matched images in the dual-image mode, with the F160W image as the detection image. Photometry in ground-based and IRAC images, whose resolutions are much lower than that of the F160W images, was measured by using **TFIT** (Laidler et al. 2007), which fit the

PSF-smoothed high-resolution image templates to the low-resolution images to measure the fluxes in the low-resolution images. We refer readers to Guo et al. (2013) and Galametz et al. (2013) for details on these data and reduction.

Photometric redshifts were estimated from a variety of different codes available in the literature, which are then combined to improve the individual performance (Dahlen et al. 2013). Rest-frame total magnitudes were computed from the best available redshifts (spectroscopic or photometric) and multi-wavelength photometry using **EAZY** (Brammer et al. 2008). Stellar masses were computed using **FAST** (Kriek et al. 2009) and based on a grid of Bruzual & Charlot (2003, BC03) models that assume a Chabrier (2003) IMF, solar metallicity, exponentially declining star formation histories, and a Calzetti et al. (2000) dust extinction law. SFRs were computed by combining IR and rest-frame UV (uncorrected for dust extinction) luminosities (Kennicutt 1998 and Bell et al. 2005) and adopting a Chabrier IMF: $\text{SFR}_{\text{IR+UV}} = 1.09 \times 10^{-10} (L_{\text{IR}} + 3.3L_{2800})$. Total IR luminosities ($L_{\text{IR}} \equiv L[8 - 1000\mu\text{m}]$) were derived from Chary & Elbaz (2001) templates fitting *MIPS* $24\mu\text{m}$ fluxes. For galaxies undetected by *MIPS* below a 2σ level ($20\mu\text{Jy}$), SFRs come from rest-frame UV luminosities at $\lambda \approx 2800\text{\AA}$ that are corrected for extinction by assuming a Calzetti law ($A_{2800} \approx 1.79A_V$) with the median A_V from all methods in Santini et al. (2015). Effective radius along the major axis (r_e) was measured from the *HST*/WFC3 F160W and F125W images respectively using **GALFIT** (Peng et al. 2002) and PSFs created and processed to replicate the conditions of the observed data (van der Wel et al. 2012).

The *HST* based multi-wavelength and multi-aperture photometry catalogs with improved local background subtraction were built for galaxies in the CANDELS fields (Liu et al. in prep.), which include the radial profiles of observed surface brightness and cumulative magnitude in the *HST*/WFC3 (F105W, F125W, F140W, and F160W) bands and *HST*/ACS (F435W, F606W, F775W, F814W and F850LP) bands if available. Part of these data has been used in recent works by Barro et al. (2015a,b). For this work, we computed the rest-frame *NUV* and *B* band surface brightness profiles, stellar mass profiles, and the profiles of other stellar population parameters (i.e., A_V , UV-based SFR, etc.) by fitting the best-fit SEDs in each photometry bin. The modeling is also based on a grid of BC03 models that assume a Chabrier IMF, solar metallicity, exponentially declining star formation histories, and a Calzetti extinction law. Note that the reddest filter in our radial data is limited to H(F160w). An extensive study by Wang et al. (in prep.) will establish that reasonable A_V values can be derived out to $z \sim 1.5$. The multi-band *HST* mosaics were PSF-matched to the resolution of F160W that has a half width at half maximum of $\text{HWHM}=0.09''$, which corresponds to ~ 0.73 kpc on average in our redshift range. In order to compensate for the light smeared outside 1 kpc of galaxies due to PSF smoothing, we followed Barro et al. (2015b) to add a Sérsic dependent correction to derived central stellar mass surface density

within a radius of 1 kpc (Σ_1).

3. Sample Selection

The full GOODS-S and UDS catalogs contain 34,930 and 35,932 objects, respectively. The sample used in this work is constructed by applying the following cuts to the above data:

1. Observed F160W magnitude $H < 24.5$ and the quality flag = 0 (van der Wel et al. 2012) to ensure well-constrained GALFIT measurements and eliminate doubles, mergers, and disturbed objects.
2. Photometry quality flag PhotFlag = 0 to exclude spurious sources
3. SExtractor CLASS_STAR < 0.9 to reduce contamination by stars
4. Redshifts within $0.5 < z < 1.5$ and stellar masses at $\log M_*/M_\odot > 9.0$ to maintain mass completeness
5. Well-constrained measurements of surface brightness profiles at least in two of *HST*/ACS bands and two of *HST*/WFC3 bands simultaneously to guarantee the accuracy of best-fit SEDs
6. Axis ratio $b/a > 0.5$ to remove galaxies with significant interplay of dust reddening and stellar population changes
7. $r_e > 0.18''$ (3 pixels) to minimize the effect of PSF-matching on color gradient measurement

After the above cuts, we obtain 1,905 galaxies: 1,008 from GOODS-S and 897 from UDS. We then utilize rest-frame *UVJ* diagram ($(U - V) > 0.88 \times (V - J) + 0.49$, Williams et al. 2009) to select 1,606 SFGs (see left panels in Figure 1). Furthermore, we follow the method of Fang et al. (in prep.) to select galaxies near the ridge-line of the star-forming main-sequence (SFMS). Right panels in Figure 1 show the SSFR-mass relation for selected galaxies. Only galaxies defined as star-forming by the *UVJ* criterion are included. As can be seen, the distributions of points clearly trace out the SFMS at these redshifts (e.g., Whitaker et al. 2012 and reference therein), while the “green-valley” galaxies appear as the tails of objects below the MS. The solid lines indicate the adopted best-fit linear relation ($\log \text{SSFR} = -0.093(\log M_* - 10) - 8.857$) to galaxies in our redshift range, after excluding “green-valley” galaxies, defined as galaxies with vertical offsets from the best-fit relation of $\Delta \log \text{SSFR} < -0.45$ dex (below dashed lines). Our choice to exclude such “green-valley”

objects is due to significant decrease in their number at low mass galaxies after the size and axis-ratio cuts, which is not sufficient for a statistically robust analysis. We will study these galaxies in the future with a large sample assembled from all five CANDELS fields. The present paper focuses on the 1,432 the main-sequence SFGs.

4. Measurements of Color Gradients

Radial surface brightness profiles along the major axis in all available *HST* bands for our galaxies were obtained. Rest-frame *NUV* and *B* band surface brightness profiles were computed using **EAZY** (Brammer et al. 2008). A linear least-squares method was then adopted to fit the derived *NUV* – *B* color profiles. To reduce PSF effect, an inner radius of 0."09 cut was used when fitting. As the data became quite noisy at large radius, the outer radius was cut at $2r_e$ to ensure errors lower than 0.1 mag *arcsec*⁻² in all bands. Consistent with previous studies (e.g., Peletier et al. 1990; Wu et al. 2005), the color gradient was expressed as $\nabla(NUV - B) \equiv d(NUV - B)/d\log(r)$. The color gradients computed by this definition are tightly correlated with color difference between inner ($r < r_e$) and outer ($r_e < r < 2r_e$) parts. We prefer such definition because it can reflect intrinsic slope in a color profile when considering the difference in radius. Figure 2 illustrates our measurement for an example galaxy (GOODS-S 16617). The color gradient in this example galaxy has a negative value (-0.37), which indicates a redder center (vice versa). The typical uncertainty in our color gradients is ~ 0.1 dex, which includes the fitting error and the errors of photometry (i.e., readout noise, sky subtraction, and PSF matching, etc.).

5. Results and Analysis

Figure 1 presents the rest-frame *UVJ* diagram (left panels) and SSFR-mass relation (right panels) for our MS SFGs at $0.5 < z < 1.5$, which are shown with points color-coded by the global A_V (top panels) and $\log\Sigma_1$ (bottom panels), respectively. In this plot, we can find the following information:

1. Bottom-right panel shows that Σ_1 and stellar mass have a tight positive correlation (also see Barro et al. 2015b), which implies that more massive galaxies may harbour larger bulges and thus tend to have denser centers, since Σ_1 is a powerful parameter to quantify the bulge growth as galaxies evolve (e.g., Fang et al. 2013).

2. Fang et al. (in prep.) have found that the reddening contours in *UVJ* diagram run nearly vertically for MS SFGs, as shown in our top-left panel, which demonstrates that

reddening correlates most strongly with $V - J$. The bottom-left panel indicates that more centrally compact galaxies are globally more dust extinguished.

3. More centrally compact galaxies are globally redder in both $U - V$ and $V - J$, likely due to a combination of increased dust reddening and buildup of larger, older bulges in the centers.

The upper panels in Figure 3 replot the UVJ diagram (left) and SSFR-mass relation (right) for our galaxies, but this time the data are binned and color-coded by raw dust-reddened $NUV - B$ color gradients as observed ($\nabla_{obs}(NUV - B)$). Direct correlations with stellar masses, Σ_1 , and rest-frame $V - J$ colors are shown in the upper panels in Figure 4 (color-coded by stellar mass). We find that the MS SFGs at $0.5 < z < 1.5$ generally have negative $NUV - B$ color gradients (redder centers). The correlations with stellar mass and Σ_1 imply that more massive and centrally compact galaxies tend to have more negative gradients. The correlation with $V - J$ indicates that galaxies also tend to have more negative color gradients with increased dust reddening.

In order to further understand the origin of negative $NUV - B$ color gradients observed in these actively SFGs, we attempt to remove dust effect by making a correction for derived $NUV - B$ color profiles and re-compute the dust-corrected gradients ($\nabla_{dc}(NUV - B)$). This correction exploits derived A_V profiles by fitting the optical-SEDs in each photometry bin and also assumes a Calzetti law ($A_{NUV} \approx 1.79A_V$ and $A_B \approx 1.26A_V$). The results are shown in the bottom panels in Figure 3 and Figure 4. It can be seen, after our correction for dust reddening, rest-frame $NUV - B$ color gradients in the low-mass ($M_* < 10^{10} M_\odot$) galaxies generally become quite flat, which implies that dust reddening is likely the principal cause of negative $NUV - B$ color gradients in the low-mass galaxies. The neutral dust-corrected $NUV - B$ color gradients also imply that these low-mass galaxies are building up their stellar masses in a self-similar way, irrespective of the radial distance. However, most of the high-mass ($M_* > 10^{10.5} M_\odot$) galaxies still retain shallow negative $NUV - B$ color gradients after correcting for dust. The buildup of compact, old bulges in their centers is likely responsible for such residual color gradients. Therefore, both increased dust reddening and presence of compact, old bulges in the centers are likely the origins of negative $NUV - B$ gradients in the high-mass galaxies. The negative dust-corrected $NUV - B$ color gradients in these high-mass galaxies are consistent with an inside-out growth scenario.

6. Discussion and Conclusions

In this Letter, we have measured the rest-frame $NUV - B$ color gradients in ~ 1400 large ($r_e > 0.''18$), face-on ($b/a > 0.5$) SFGs near the ridge-line of the MS between redshift 0.5 and 1.5 in the CANDELS/GOODS-S and UDS fields. With this sample, we for the first time make a statistically robust analysis of UV-optical color gradients in actively SFGs at $z \sim 1$. Since the rest-frame UV-optical color index is sensitive to SSFR and dust extinction, but insensitive to the metallicity, we corrected for dust extinction to disentangle the effects. Our main conclusions are as follows:

1. Both massive and centrally compact SFGs are globally more dust extinguished.
2. More massive, centrally compact and more dust extinguished SFGs tend to have more negative raw $NUV - B$ color gradients than less massive, centrally diffuse and less dusty SFGs.
3. After correcting for dust reddening, the $NUV - B$ color gradients in the low-mass ($M_* < 10^{10} M_\odot$) SFGs generally become quite flat, while most of the high-mass ($M_* > 10^{10.5} M_\odot$) SFGs still retain shallow $NUV - B$ negative gradients. These findings imply that dust reddening is likely the principal cause of negative color gradients in the low-mass SFGs, whereas both increased dust reddening and buildup of compact, old bulges in the centers are likely the origins of negative color gradients in the high-mass SFGs.
4. The neutral dust-corrected $NUV - B$ color gradients in the low-mass SFGs imply that their stellar masses grow self-similarly at all radii. The negative dust-corrected $NUV - B$ color gradients in the high-mass SFGs imply that central stars form earlier than outer stars, i.e., that massive galaxies are growing from inside out.

Recently, van der Wel et al. (2014) showed that the low-mass galaxies at these redshifts are not disk-like but are prolate and irregular, unlike massive galaxies, which are shaped like normal, oblate disks. A consistent picture with our data is emerging in which young, low-mass galaxies first grow in an irregular manner, where new generations of stars are randomly mixed with previously existing populations, and that inside-out growth only occurs once galaxies attain a sustained, disk-like structure. Assuming that our fourth conclusion persists over a substantial range of redshifts, we infer that star-forming galaxies start out their lives growing self-similarly in their early phases and switch to growing from inside out when their masses pass $M_* \sim 10^{10} M_\odot$. Since centers appear redder (older) after that, the change must happen because the centers slow down rather than the reverse (having the outer regions accelerate). This change marks the entry into the later stages of star-formation and signals incident entry into the transition region (green valley), followed by quenching. It will be useful to use galaxy formation models to put actual time markers on these various stages.

We stress that major conclusions in this paper depend on the SED modeling assumptions applied to the CANDELS data, namely (1) that galaxy stellar populations are single τ -models, (2) that the dust extinction law is assumed to be the Calzetti, and (3) that the solar metallicity applies to all galaxies. These standard assumptions are what almost all of high- z studies are currently using. This paper does not attempt to justify these current state of the art assumptions, but take the standard assumptions as given and aims to see where they lead. We refer to the reader to Fang et al. (in prep.) about the uncertainties introduced by these standard assumptions. Future works should investigate the consequences of more realistic stellar population models, metallicity, and extinction law.

We thank Chenggang Shu and Zhu Chen for useful discussions. We acknowledge the anonymous referee for a constructive report that significantly improved this paper. This project was supported by the NSF grants of China (11103013, 11573017).

REFERENCES

- Barro, G., Faber, S. M., & Dekel, A., et al. 2015a, ArXiv e-prints:1503.07164
- Barro, G., Faber, S. M., & Koo, D. C., et al. 2015b, ArXiv e-prints:1509.00469
- Bell, E. F., Papovich, C., et al. 2005, ApJ, 625, 23
- Bertin, E. & Arnouts, S. 1996, A&AS, 117, 393
- Brammer, G. B., van Dokkum, P. G., & Coppi, P. 2008, ApJ, 686, 1503
- Bruzual, G. & Charlot, S. 2003, MNRAS, 344, 1000
- Calzetti, D., Armus, L., Bohlin, R. C., Kinney, A. L., Koornneef, J., & Storchi-Bergmann, T. 2000, ApJ, 533, 682
- Chabrier, G. 2003, PASP, 115, 763
- Chary, R. & Elbaz, D. 2001, ApJ, 556, 562
- Dahlen, T., Mobasher, B., & Faber, S. M., et al. 2013, ApJ, 775, 93
- Fang, J. J., Faber, S. M., Koo, D. C., & Dekel, A. 2013, ApJ, 776, 63
- Galametz, A., Grazian, A., Fontana, A., & the CANDELS Team. 2013, ApJS, 206, 10
- Gonzalez-Perez, V., Castander, F. J., & Kauffmann, G. 2011, MNRAS, 411, 1151

- Grogin, N. A., Kocevski, D. D., & Faber, S. M., et al. 2011, *ApJS*, 197, 35
- Guo, Y., Ferguson, H. C., & Giavalisco, M., et al. 2013, *ApJS*, 207, 24
- Guo, Y., Giavalisco, M., Cassata, P., et al. 2011, *ApJ*, 735, 18
- Kaviraj, S., Rey, S.-C., Rich, R. M., Yoon, S.-J., & Yi, S. K. 2007, *MNRAS*, 381, L74
- Kennicutt, Jr., R. C. 1998, *ARA&A*, 36, 189
- Kobayashi, C. & Arimoto, N. 1999, *ApJ*, 527, 573
- Koekemoer, A. M., Faber, S. M., & Ferguson, H. C., et al. 2011, *ApJS*, 197, 36
- Kriek, M., van Dokkum, P. G., Labbé, I., Franx, M., Illingworth, G. D., Marchesini, D., & Quadri, R. F. 2009, *ApJ*, 700, 221
- Laidler, V. G., Papovich, C., & Grogin, N. A., et al. 2007, *PASP*, 119, 1325
- Nelson, E. J., van Dokkum, P. G., et al. 2012, *ApJ*, 747, L28
- Nelson, E. J., van Dokkum, P. G., et al. 2015, arXiv:1507.03999
- Nelson, E. J., van Dokkum, P. G., et al. 2016, *ApJ*, 817, L9
- Pan, Z., Li, J., Lin, W., Wang, J., Fan, L., & Kong, X. 2015, *ApJ*, 804, L42
- Peletier, R. F., Davies, R. L., Illingworth, G. D., Davis, L. E., & Cawson, M. 1990, *AJ*, 100, 1091
- Peng, C. Y., Ho, L. C., Impey, C. D., & Rix, H.-W. 2002, *AJ*, 124, 266
- Santini, P., Ferguson, H. C., & Fontana, A., et al. 2015, *ApJ*, 801, 97
- Suh, H., Jeong, H., Oh, K., Yi, S. K., Ferreras, I., & Schawinski, K. 2010, *ApJS*, 187, 374
- Tamura, N. & Ohta, K. 2003, *AJ*, 126, 596
- Tortora, C., Napolitano, N. R., Cardone, V. F., Capaccioli, M., Jetzer, P., & Molinaro, R. 2010, *MNRAS*, 407, 144
- van der Wel, A., Bell, E. F., & Häussler, B., et al. 2012, *ApJS*, 203, 24
- van der Wel, A., Chang, Y.-Y., Bell, E. F., et al. 2014, *ApJ*, 792, L6
- van der Wel, A., Franx, M., & van Dokkum, P. G., et al. 2014, *ApJ*, 788, 28

Whitaker, K. E., van Dokkum, P. G., Brammer, G., & Franx, M. 2012, *ApJ*, 754, L29

Williams, R. J., Quadri, R. F., Franx, M., van Dokkum, P., & Labbé, I. 2009, *ApJ*, 691, 1879

Wu, H., Shao, Z., Mo, H. J., Xia, X., & Deng, Z. 2005, *ApJ*, 622, 244

Wuyts, S., et al. 2012, *ApJ*, 753, 114

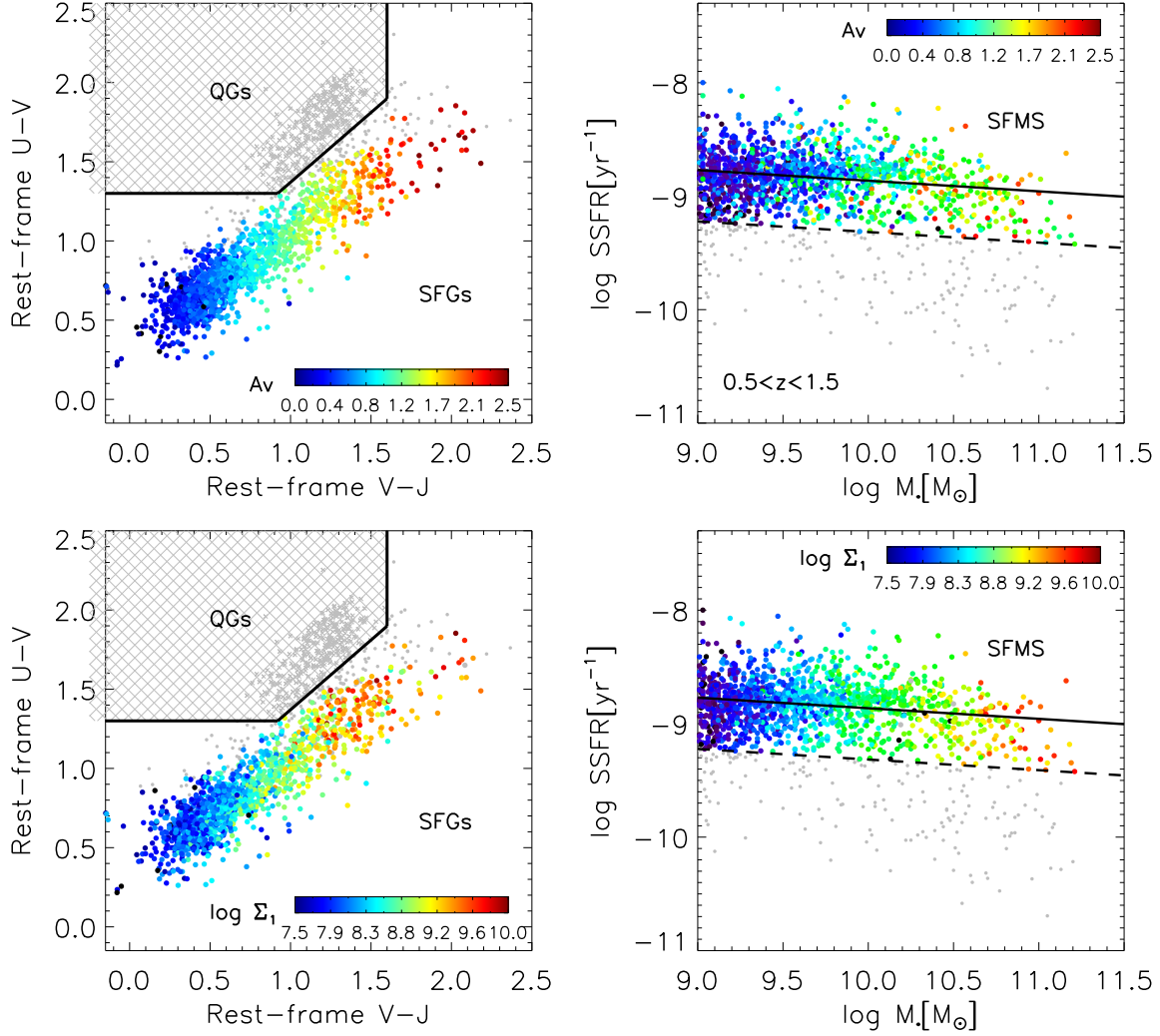


Fig. 1.— Rest-frame global UVJ diagram (left) for our sample galaxies after applying the selection cuts (see §1) and SSFR vs. stellar mass (right) for only UVJ -defined star-forming galaxies. Quiescent galaxies are shown with gray hatching in the left panels. The solid lines in the left panels indicate the selection criterion provided by Williams et al. (2009). The solid lines in the right panels show the best linear relation to the SFMS in our adopted redshift range. The “green-valley” galaxies, defined to have residuals $\Delta \log \text{SSFR} < -0.45$ dex (below dashed lines) are shown with gray solid points. Points for main-sequence SFGs are color-coded by the global A_V (top panels) and $\log \Sigma_1$ (bottom panels), respectively.

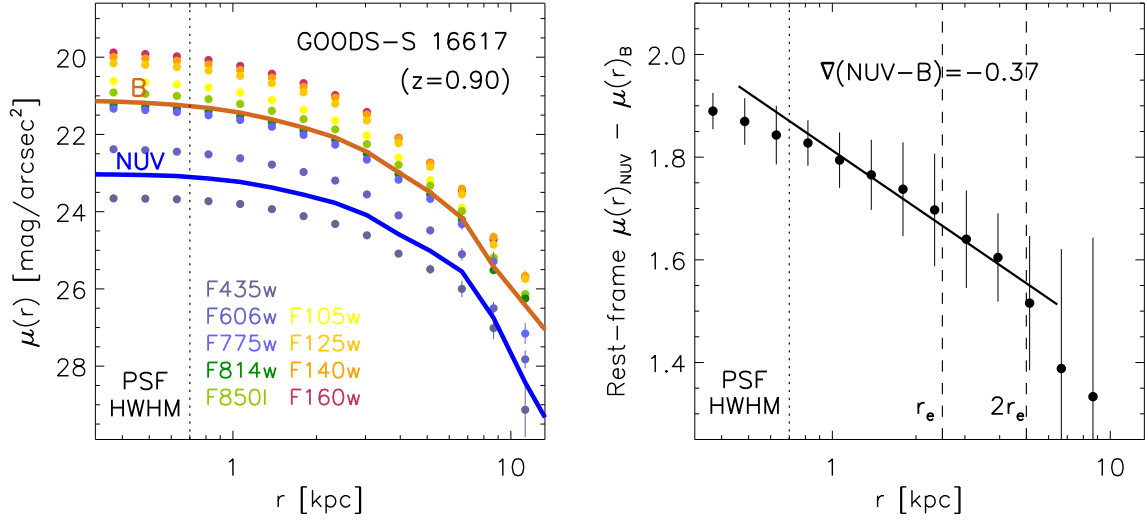


Fig. 2.— Example galaxy GOODS-S 16617 illustrating our measurement of rest-frame $NUV - B$ color gradient. The observed *HST* multi-band surface brightness profiles and derived rest-frame NUV and B band surface brightness profiles are shown in the left panel. Rest-frame $NUV - B$ color profile and the best linear fit are shown in the right panel.

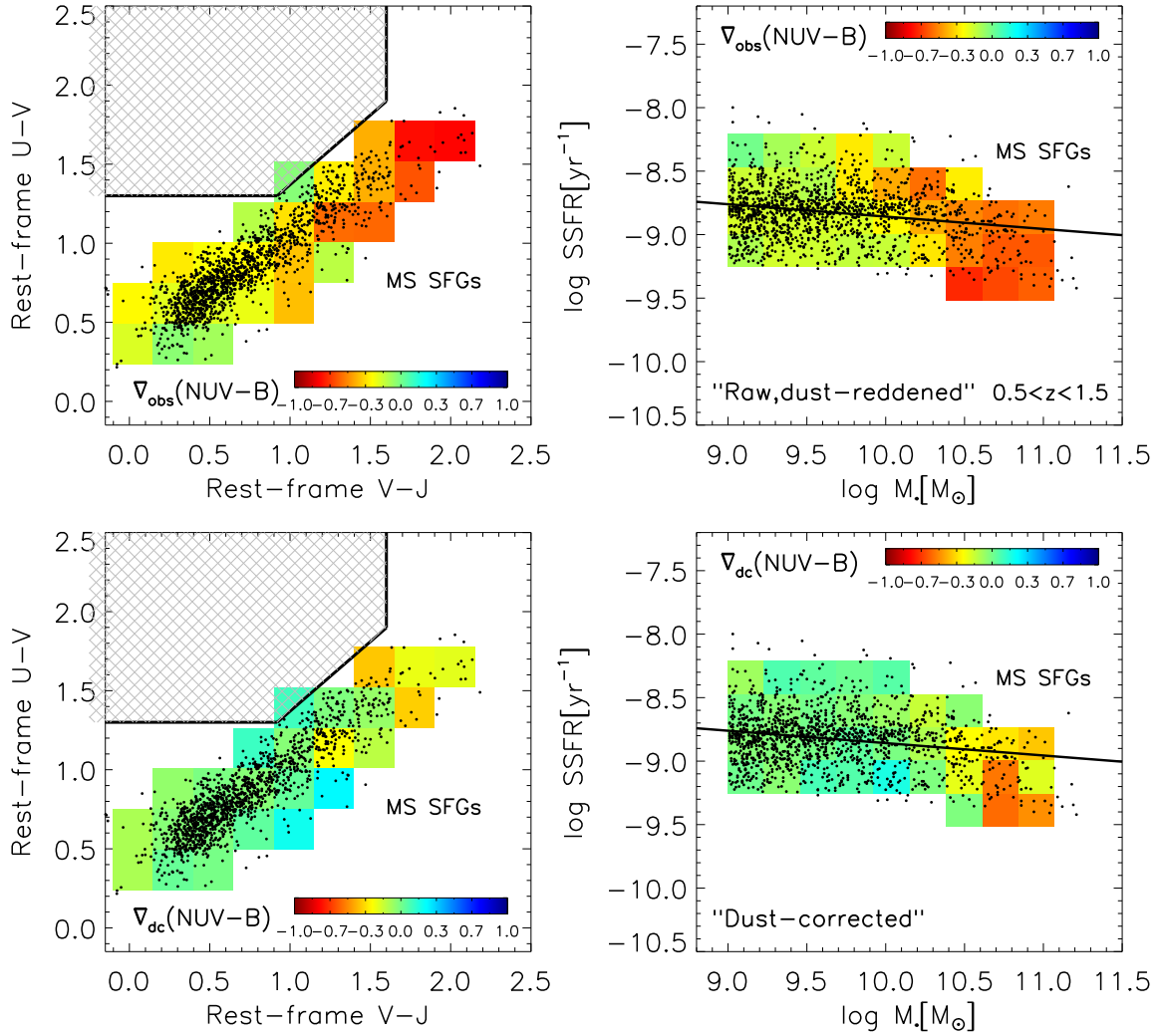


Fig. 3.— Rest-frame global UVJ diagram (left) and SSFR vs. stellar mass (right) for the main-sequence SFGs used in this study. Points are binned and color-coded by raw dust-reddened $NUV - B$ color gradients as observed (top panels) and dust-corrected $NUV - B$ color gradients (bottom panels), respectively.

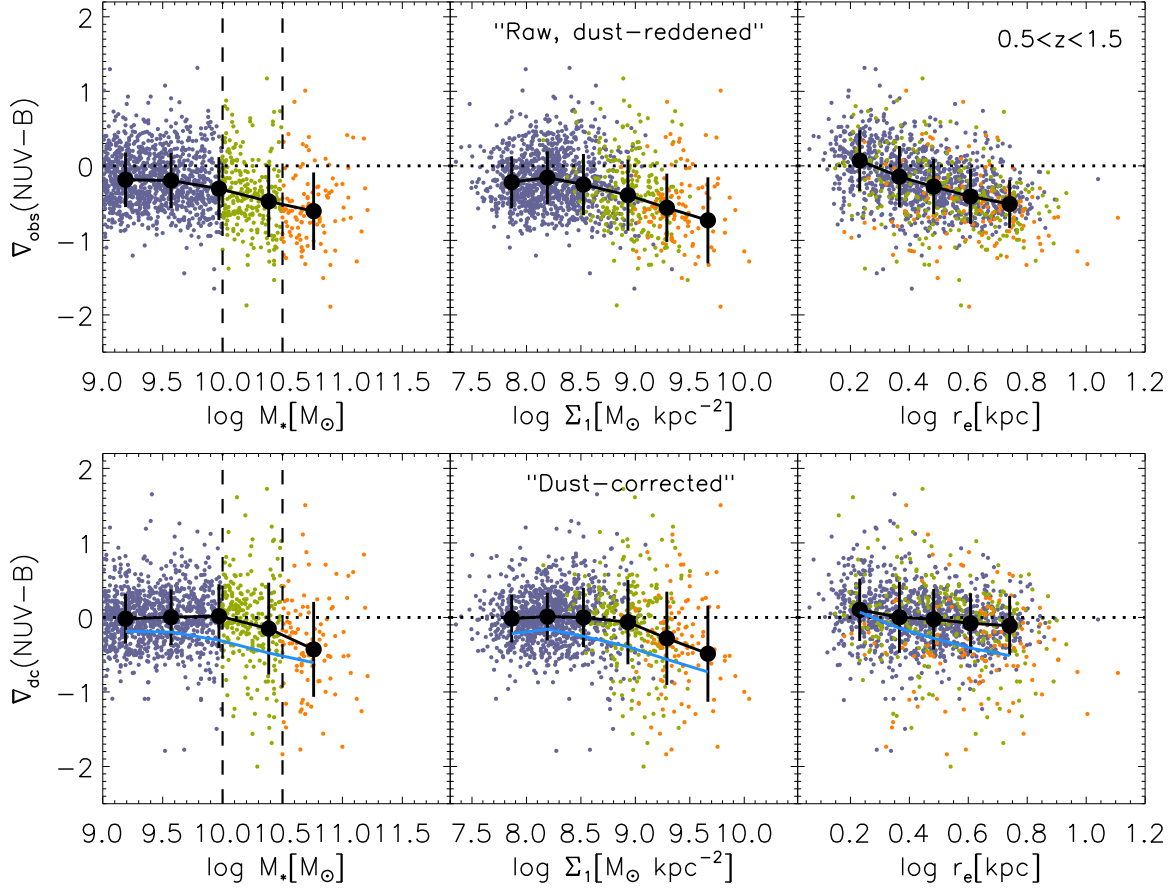


Fig. 4.— Raw dust-reddened (as observed, upper panels) and dust-corrected (bottom panels) rest-frame $NUV - B$ color gradients in the main-sequence SFGs at $0.5 < z < 1.5$ as a function of their stellar masses, Σ_1 and rest-frame $V - J$ colors from left to right, respectively. The median values and corresponding standard deviations in classified bins in each panel are shown with black symbols. The trends for the correlations in the upper panels overlay the lower panels with blue solid lines. The horizontal dotted lines indicate zero gradients. The sample galaxies are divided into three mass subgroups ($M_* < 10^{10} M_\odot$, $10^{10} M_\odot < M_* < 10^{10.5} M_\odot$ and $M_* > 10^{10.5} M_\odot$), which are shown with different colors, respectively.